JOURNAL OF MATERIALS SCIENCE 37 (2002) 567–575

Densification and strength evolution in solid-state sintering

Part I *Experimental investigation*

XIAOPING XU, WUWEN YI, RANDALL M. GERMAN
Center for Innovative Sintered Products, P/M Lab, 147 Research West, Pennsylvania State University, University Park, PA 16802-6809 USA
E-mail: rmg4@psu.edu

Prealloyed bronze (Cu-10Sn) powder and a mixed elemental steel (Fe-2Ni-0.9C) powder were evaluated for strength evolution during sintering. For the bronze powder, test samples were fabricated using a loose powder casting method, while the steel powder was formed by injection molding. *In situ* strength during sintering was measured using a bending fracture test. Primary focus was on measuring the effects of sintering temperature and time on *in situ* strength evolution. Sintering temperature had the most significant effect, but the strength underwent significant gains prior to densification. The results are explained by the competition among interparticler neck growth, densification, and thermal softening. Sinter strengthening is initially governed by interparticle bonding, followed by a contribution from densification at high temperatures. However, high temperatures also lead to significant strength degradation due to thermal softening. Densification is favored by the declining *in situ* strength associated with thermal softening at high temperatures.
© *2002 Kluwer Academic Publishers*

1. Introduction

Powder metallurgy has the ability to fabricate high quality, complex components to close tolerances in an economical manner [1]. The net-shaping capacity of the technique dictates precise dimensional control to eliminate post-sintering operations. Although a high sintered density is desired in many applications, sintering to full density demands a large shrinkage, often resulting in difficulties with dimensional control. Loss of dimensional control can occur at low temperatures due to the low strength of the green body. For example, warping and even cracking occur from stresses generated by gravity, substrate friction, thermal gradients, or green density inhomogeneities that induce stresses that exceed the *in situ* strength of the component [2]. Also, distortion occurs at high temperatures when the compact is weak, typically near the point of full densification. Thus, understanding *in situ* strength evolution is important to minimize loss of dimensional precision in sintering. Unfortunately, lack of knowledge on strength evolution inhibits heating cycle design for improved dimensional control.

This study investigates important parameters affecting sinter strengthening, including interparticle bonding, densification, and thermal softening. Interparticle bonding dominates sinter strengthening during initial heating, followed by a strength contribution from densification at high sintering temperatures. On the other hand, high temperatures significantly degrade strength due to thermal softening of the bulk material. Therefore, the *in situ* strength evolution in sintering is determined by the competition among several events.

2. Experimental procedures

Prealloyed bronze (Cu-10Sn) and mixed elemental steel (Fe-2Ni-0.9C) powders were selected in this study. The prealloyed bronze was used as a model system because of its simple chemistry, relative low sintering temperature, and near spherical particle shape. Table I gives the bronze powder characteristics, including the source, particle size distribution, surface area, and packing densities. Fig. 1 shows a SEM image of the spherical as-received bronze powder. The starting Fe-2Ni-0.9C steel was a premixed feedstock for powder injection molding, as characterized in Table II [3].

Transverse rupture bars (TRBs) of bronze were made using a powder casting method. Bronze powder was mixed with a solution consisting of 240 g powder, 35 ml distilled water, 0.8 g polysaccharide (Gallen Gum, Kelco, San Diego, CA), and 1 drop of polyethylene glycol-200. The samples were 32 to 33 mm long, 10 to 12 mm wide, and 7 to 9 mm thick with a green fractional density of $55 \pm 1\%$. To gain handling strength, the green bronze samples were presintered at 600°C in hydrogen for 120 min with no measurable change in density.

The transverse rupture bars for the steel composition were fabricated by injection molding using the parameters listed in Table III [3]. The binder is 90-wt%

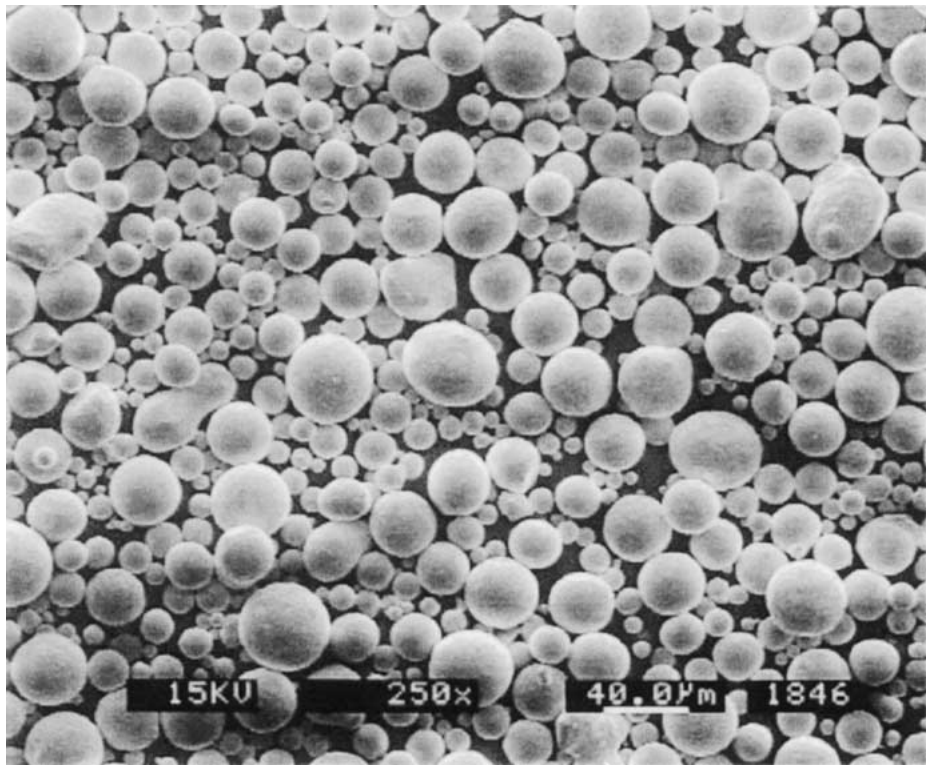

Figure 1 SEM image of prealloyed Cu-10Sn bronze powder showing spherical particle shape.

TABLE I Powder characteristics for the prealloyed Cu-10Sn bronze

Powder	Bronze
Vendor	ACuPowder International
Designation	10P
Apparent density, g/cm^3	5.0
Tap density, g/cm^3	5.7
Pycnometer density, g/cm^3	8.9
BET surface area, m^2/g	0.04
Size distribution, μm	
D_{10}	10.0
D_{50}	17.9
D_{90}	30.4
Mean	19.4

TABLE II Feedstock characteristics for the mixed elemental steel (Fe-2Ni-0.9C) system [3]

Feedstock	Catamold Fe-2Ni
Vendor	BASF
Fe particle size	$D_{10} = 1.5\,\mu$m
	$D_{50} = 3.9\,\mu$m
	$D_{90} = 10.1\,\mu$m
Carbon content	0.9 wt%
Oxygen content	0.3 wt%
Feedstock size	Approximately 3 mm^3
Density of feedstock	4.98 ± 0.06 g/cm^3
Solid volume fraction	0.57
Solid weight percent	91.6%
Melt temperature	185°C

TABLE III Injection molding parameters for the steel feedstock

Parameter	Value				
Nozzle temperature, °C			193		
Barrel temperature, °C	189		189		185
Heating zones	1		2		3
Mold temperature, °C			120		
Screw speed control					
Injection profile position, mm	71.1	60.2	58.7	56.4	54.6
Speed, mm/s	152.4	203.2	127.0	20.3	2.5
Pressure control					
Packing pressure, MPa	10.7	9.3	6.6	2.4	5.2
Profile step number	1	2	3	4	5
Packing hold time, s			9		
Cooling time, s			45		
Screw back pressure, MPa			0.2		

polyacetal and 10-wt% polyolefin, requiring a two-step debinding process. The polyacetal phase was catalytically removed at 140°C using flowing nitrogen doped with nitric acid as a catalyst, while the polyolefin was thermally extracted by heating to 500°C in hydrogen prior to sintering. Similar sized steel TRBs were fabricated via powder injection molding with a 57% solid green density.

In situ transverse rupture strengths were measured using the Flaming Tensile Tester (FTT) sketched in Fig. 2 at a displacement rate of 1 mm/s. For bronze, the *in situ* strength was measured at temperatures up to 850°C with hold times of 0, 30, 60, and 180 min at testing temperatures of 600°C, 700°C, or 800°C. The sintering atmosphere was dry hydrogen with a drew point below −40°C. Four sets of cooling experiments were conducted to investigate the thermal softening behavior. For the cooling experiments, TRBs were first sintered in pure hydrogen for 180 min in a CM horizontal tube furnace. The heating rate was 5°C/min to temperatures of 600, 700, 750, or 800°C. The sintered bars were then reheated at 10°C/min in pure hydrogen to test temperatures between room temperature and the

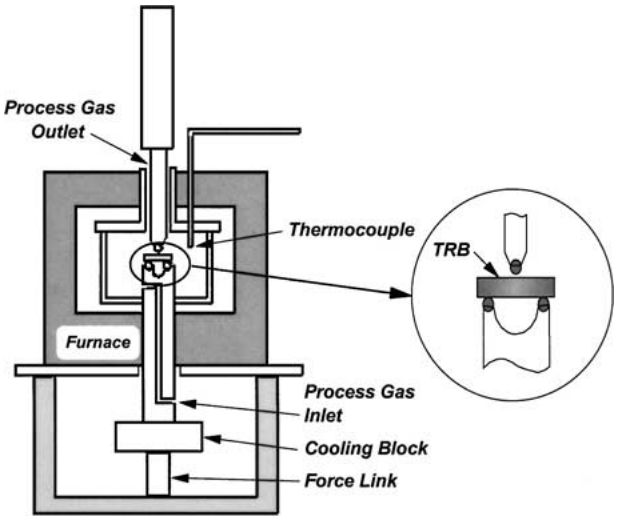

Figure 2 A section view of the Flaming Tensile Tester (FTT) used for both the *in situ* strength and post-sintering bend strength measurements.

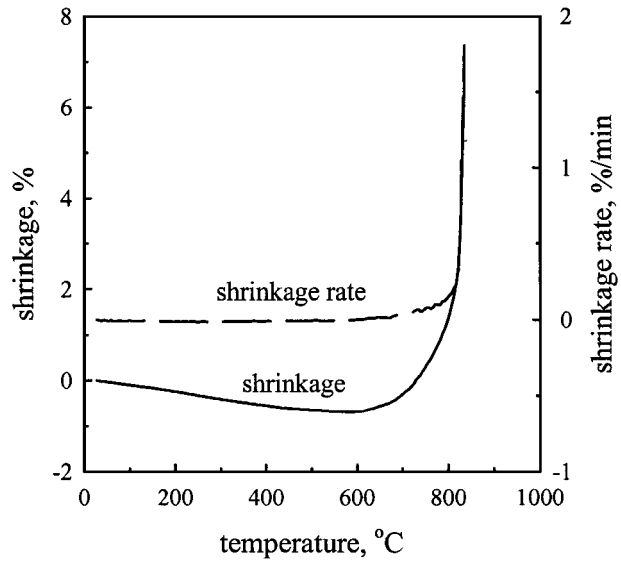

Figure 3 Dilatometer plot of shrinkage and shrinkage rate versus temperature for the Cu-10Sn bronze powder heated at 5°C/min in hydrogen.

peak sintering temperature to conduct the strength tests. Sintered strength of bronze was also measured at room temperature in the FTT. The transverse rupture strength is calculated as follows [4]:

$$\sigma_{TRS} = \frac{3PL}{2wt^2} \quad (1)$$

where P is the recorded peak fracture force, L is the 2-point support span length (25.4 mm), w is the sample width, and t is the sample thickness.

The steel *in situ* bend strength measurements were conducted at temperatures up to 1100°C in an atmosphere of 80% N_2 and 20% H_2. After cooling, the sintered bend strength was also measured using the FTT. Because these samples were ductile and Equation 1 assumes brittle fracture, the recorded proportional limit in the load-deflection curve was used to calculate the effective yield strength. For comparison, sintered tensile strength of the steel was measured using a screw-type machine with a 64 kN load frame.

After sintering and fracture, compacts were examined for interparticle sinter bonding using scanning electron microscopy (SEM). More than 100 interparticle sinter necks were imaged and sized. For each bonded particle pair, the neck size ratio was calculated by dividing the neck diameter X by the average diameter D of the two particles.

3. Experimental results

3.1. Sintering densification

To monitor shrinkage, bronze samples were heated in hydrogen at 5°C/min up to 850°C in a push-rod dilatometer. A plot showing shrinkage and shrinkage rate versus temperature is given in Fig. 3. The sample initially underwent expansion, followed by gradual shrinkage. There was no significant shrinkage rate at temperatures up to 800°C. Cumulative densification was evident at temperatures above 750°C. When the sample was heated to about 840°C, both the shrinkage and shrinkage rate showed abrupt increases as the

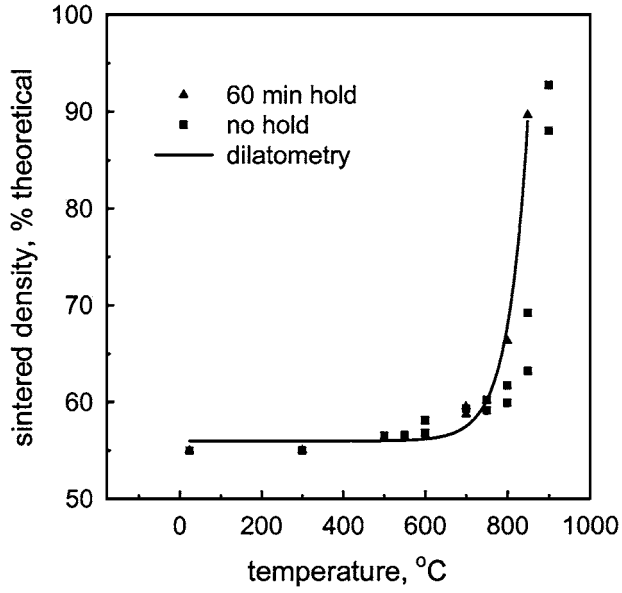

Figure 4 Sintered density versus temperature for the Cu-10Sn bronze powder. The heating rate was 5°C/min.

850°C solidus temperature was approached. A plot of sintered density versus peak temperature is shown in Fig. 4, comparing no hold and 60 min hold results with the dilatometry data. In all cases, an appreciable increase in sintered density was observed at temperatures above 750°C. The difference between dilatometry and batch sintering probably traces to the contact force from the dilatometer push rod.

Fig. 5 shows the dilatometer results for the steel powder heated to 1400°C at 5°C/min in an atmosphere of 80% N_2 and 20% H_2. As shown in Fig. 5, both the shrinkage and shrinkage rate were small below 600°C. A substantial increase in shrinkage was observed at temperatures from 600°C to 900°C, but the shrinkage rate declined above 900°C.

A plot of sintered density versus sintering temperature for the Fe-2Ni-0.9C steel is shown in Fig. 6. Note a curve of sintered density versus sintering temperature

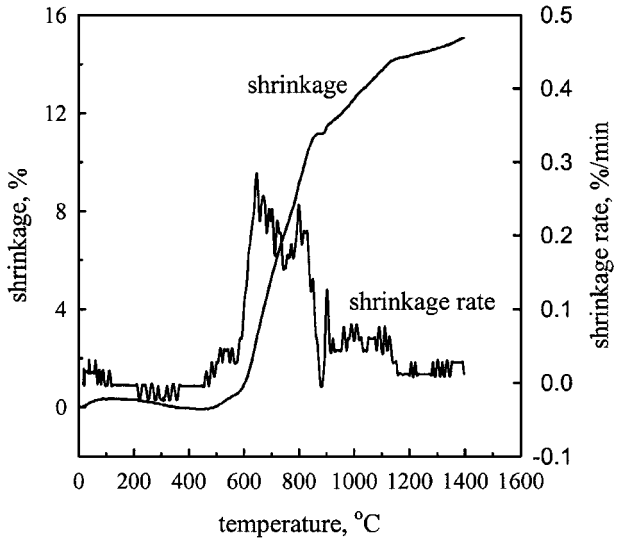

Figure 5 Dilatometer data for shrinkage and shrinkage rate versus temperature for the Fe-2Ni-0.9C steel powder heated 5°C/min in an atmosphere of 80% N_2 and 20% H_2.

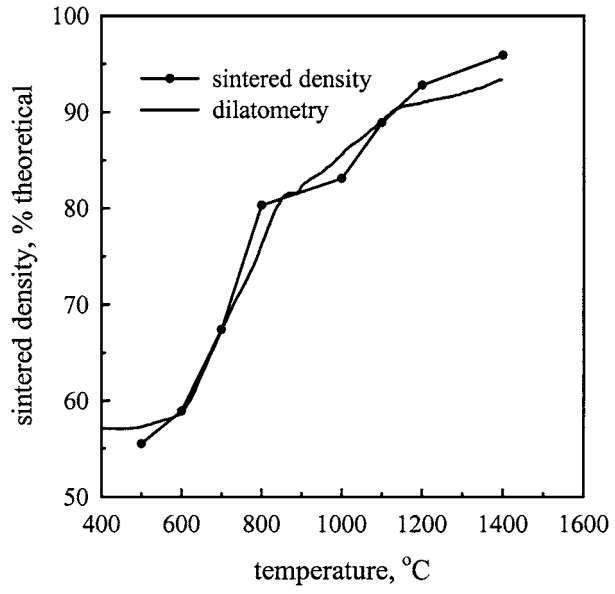

Figure 6 Sintered density versus temperature for the Fe-2Ni-0.9C steel heated at 5°C/min in an atmosphere of 80% H_2 and 20% N_2 with no hold at the peak temperature. Dilatometer data are included for comparison.

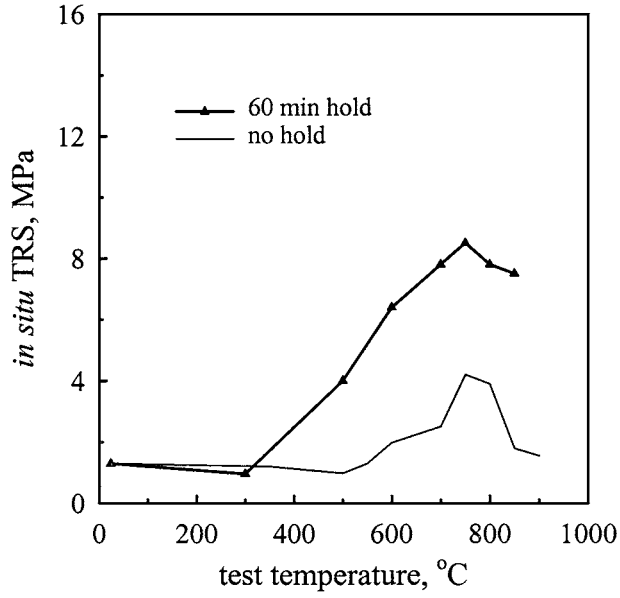

Figure 7 A plot in *in situ* transverse rupture strength versus test temperature for the Cu-10Sn bronze powder heated at 5°C/min.

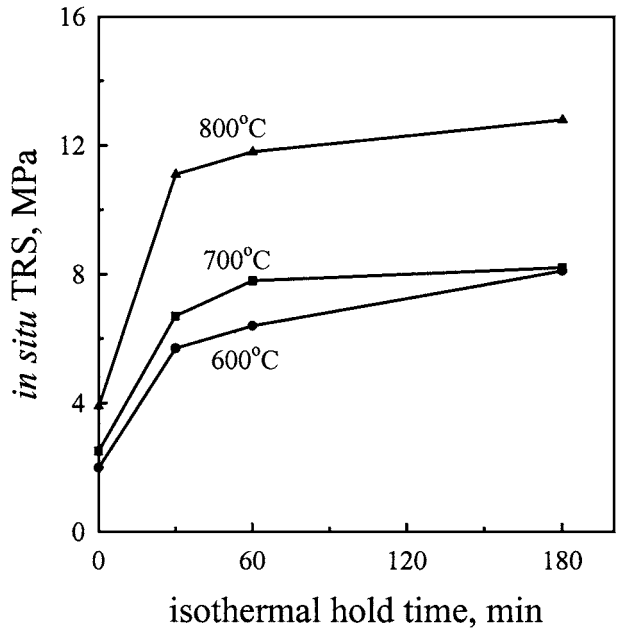

Figure 8 *In situ* transverse rupture strength versus isothermal hold time at the test temperature for the Cu-10Sn bronze powder heated at 5°C/min.

calculated from the dilatometer results is included in the figure. As evident from Fig. 6, increasing temperature was effective in promoting densification: An increase in temperature from 600°C to 800°C resulted in an increase of about 22% in sintered density. A density of about 96% was obtained by sintering at 1400°C.

3.2. Strength evolution

Fig. 7 shows *in situ* strength evolution as a function of sintering temperature for the prealloyed Cu-10Sn bronze powder. The experiments were conducted using a constant heating rate of 5°C/min in hydrogen. The green strength of the starting TRBs was 1.2 MPa. As the temperature increased, the strength decreased to about 1.0 MPa at 500°C. This reduction in strength was due to binder burnout prior to the onset of interparticle bonding. An appreciable increase in strength was observed at temperatures between 500°C and 750°C. The peak in strength occurred at 750°C at 4.1 MPa for no hold, and 8.1 MPa for the 60 min hold. Above 750°C, a further increase in temperature causes decay in strength through the highest test temperature of 900°C. To further investigate the effect of isothermal hold time on sinter strengthening, several fracture tests were conducted at test temperatures of 600°C, 700°C, or 800°C with isothermal sintering times up to 180 min. The heating rate was 5°C/min, and sintering atmosphere was pure hydrogen. Fig. 8 plots the *in situ* strength as a function of isothermal hold time for temperatures of 600°C, 700°C, and 800°C. An appreciable gain in strength was observed during the first 30 min. A prolonged hold of 180 min led to only a minor increase in strength. For

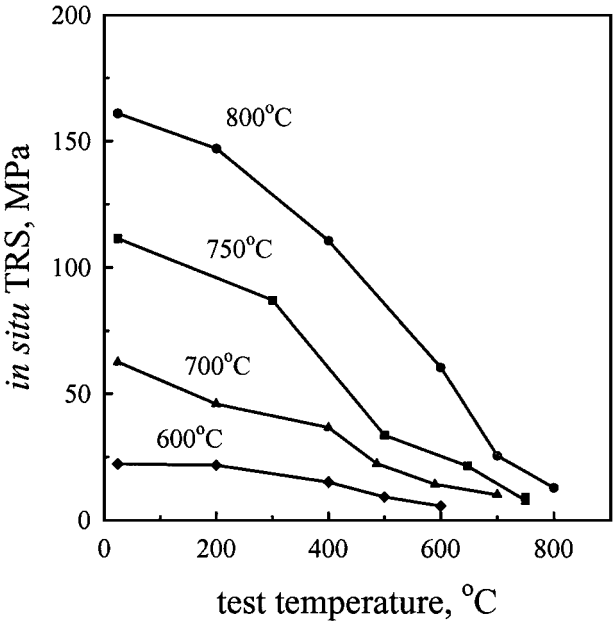

Figure 9 Thermal softening behavior of the Cu-10Sn bronze powder. The samples were sintered for 180 min at peak temperatures of 600°C, 700°C, 750°C, or 800°C. Then the samples were reheated in 100% hydrogen to each test temperature to obtain the strength measurements.

each isothermal hold time, the measured *in situ* strength increased with sintering temperature.

The effect of thermal softening was studied using cooling experiments. The samples were sintered at the peak temperatures of 600°C, 700°C, 750°C, or 800°C. A long isothermal hold time of 180 min at the peak temperatures was employed to minimize the effects of any neck growth during cooling, so that the experiments were performed based on the same neck size ratio for each peak sintering temperature. Thermal softening behavior is plotted in Fig. 9 by showing the *in situ* strength against the test temperature, showing a reduction in strength as temperature increased. For the experiments with peak sintering temperature of 800°C, the remaining *in situ* strength at 800°C was less than 10% of its room temperature strength of approximately 160 MPa. Note that for all four cases, the ratio of strength at 600°C to the room temperature strength is about one-third.

Typical scanning electron microscope images of fracture surfaces for the bronze samples are shown in Fig. 10. These images indicate progressive neck growth with an increase in sintering temperature. Only a small interparticle bond size was observed in a sample sintered at 600°C for 180 min, as identified in Fig. 10a. The fracture surface of the sample sintered at 700°C for 180 min showed an overall enlarged interparticle bond area, compared to the sample sintered at 600°C for 180 min. The obvious fracture surface tearing for the sample sintered at 800°C for 180 min indicated a high degree of interparticle bonding. With a further increase in temperature to 850°C, significant fracture surface tearing and particle deformation showed a even higher degree of interparticle bonding, as evident in Fig. 10d. Note this sample was sintered with no hold. These fracture surface images clearly indicate interparticle neck growth strongly depended on temperature.

TABLE IV The carbon content for the sintered steel samples

Sintering temperature, °C	Prior to sintering	1000	1200	1400
Carbon content, wt.%	0.90	0.93	0.89	0.91

Fig. 11 shows a plot of *in situ* bend yield strength versus temperature for the steel. The *in situ* bend yield strength decreased slightly during initial heating, followed by a continuous rapid increase with test temperature. Significant strengthening occurred between 500°C and 970°C due to interparticle neck growth and densification. The *in situ* strength peaked at about 970°C, and then decreased with a further increase in temperature. Selected sintered samples were analyzed for final carbon content to ensure the strength variation was not due to a composition change. Table IV compares the carbon contents for the initial steel and for samples sintered for 60 min at 1000°C, 1200°C, and 1400°C, respectively. The results showed no appreciable carbon change during sintering. Therefore, both *in situ* and sintered strength are determined by sinter bonding factors addressed in this study, not by carbon variations during sintering.

Fig. 12 shows a plot of sintered bend yield strength versus sintering temperature, indicating an approximately linear relation between sintered strength and temperature. Because of sample ductility during high temperature testing, the sintering parameter effects on sintered strength were examined using room temperature tensile tests. Figs 13 and 14 are plots of sintered ultimate tensile strength versus sintering temperature and hold time, respectively. As shown in these plots, sintered tensile strength increased significantly with sintering temperature in a nearly linear relation. For example, the sintering at 1000°C gives 230 MPa, but the strength increases to approximately 600 MPa following sintering at 1400°C. On the other hand, the isothermal hold did not have a substantial effect on the sintered strength. After holding at 1200°C for 60 min the strength was only 2% higher than with no hold at the same temperature.

4. Discussion

Sintering involves heating a powder to a temperature where bonding is stimulated [5]. The atomic motion leads to interparticle bonding and possible shrinkage. Interparticle bonding is generally favored during initial heating with little densification. This is evident for the bronze powder in Fig. 15, in which interparticle neck size ratio (X/D) and sintered density are plotted against sintering temperature. Densification followed behind interparticle bond growth. For example, a sample sintered at 700°C for 60 min showed an average interparticle neck size ratio of 0.33 with only 4% increase in density. Densification is observed at higher temperatures where bulk transport is active. This can be seen in the shrinkage results of Fig. 3. Both the shrinkage and shrinkage rate were small at temperatures under 750°C, followed by rapid shrinkage above 800°C. Dilatometry on a different bronze powder by Lal *et al.* [6] yielded a similar result. Shrinkage was delayed to 600°C, followed by a sudden increase above 800°C.

For the steel, the shrinkage shown in Fig. 5 indicates no densification prior to 600°C. However, an obvious increase in sintered strength, as shown in Fig. 12, demonstrated significant interparticle bond growth before densification. Sinter bonding is the result of multiple transport mechanisms. However, the dominance of each mechanism varies with temperature and sintering stage. For metals, surface diffusion is usually favored at low temperatures during heating, resulting in interparticle bonding with no shrinkage. Therefore, interparticle bonding is a primary strengthening mechanism during low temperature sintering. Heating to a high temperature, where bulk transport mechanisms are active, induces densification. Strength gains at high temperatures come from the further neck growth, densification (removal of pores), and a higher coordination number for each particle (closer packing induces more neighboring bonds).

The strength increase associated with sintering emerges from the sinter bonds between contacting grains [5]. Nyce and Shafer [7] demonstrated the key parameter is the neck size ratio of the interparticle bond, which relates to sintered strength by an empirical model as follows,

$$\sigma = A\sigma_o\left(\frac{X}{D}\right)^2 \tag{2}$$

where A is an empirical constant, σ_o is the wrought material strength, and X/D is the neck size ratio (interparticle neck diameter divided by particle diameter). Shoals and German [2] developed a phenomological

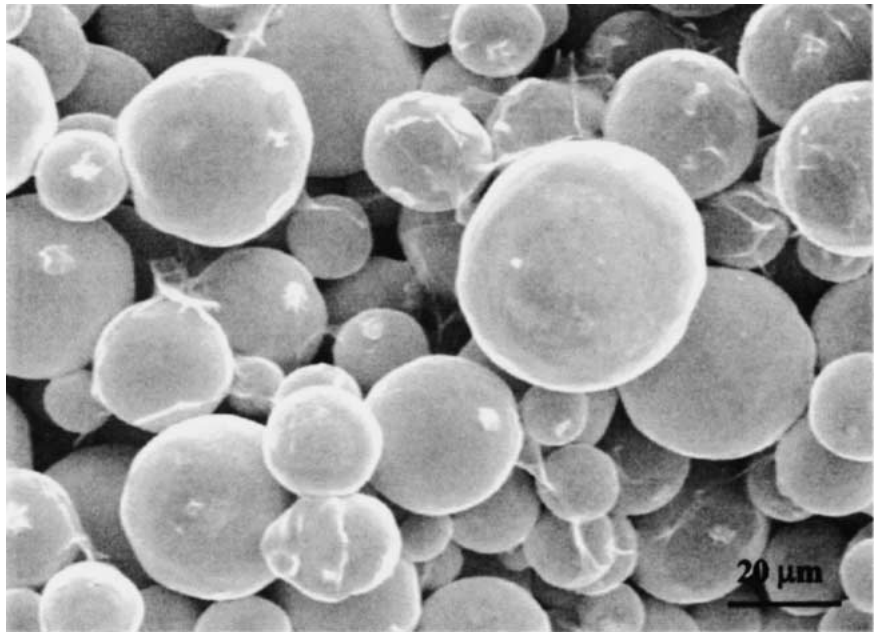

(a)

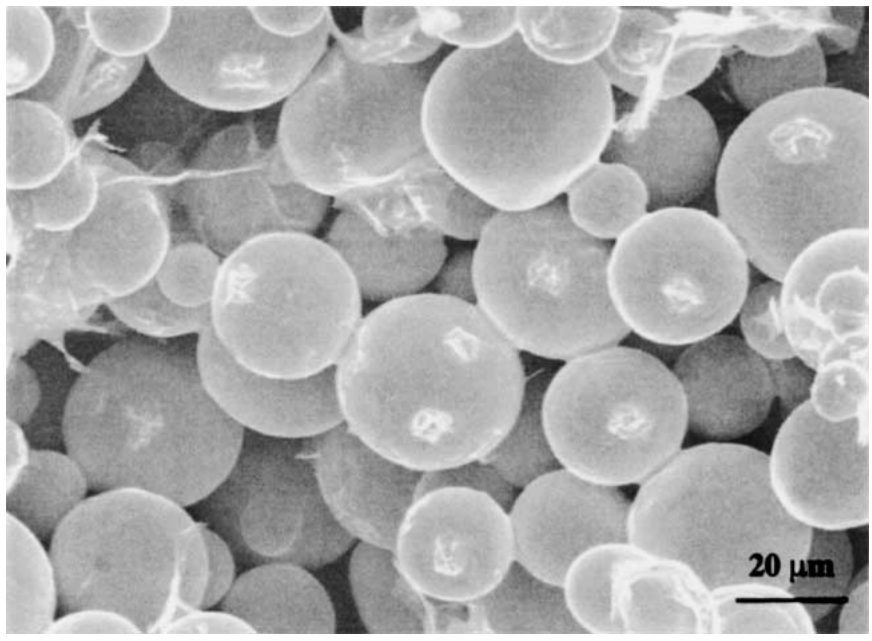

(b)

Figure 10 SEM fracture surfaces of for the Cu-10Sn bronze samples sintered under various conditions. In each case the heating rate was 5°C/min, (a) 600°C for 180 min, (b) 700°C for 180 min, (c) 800°C for 180 min, and (d) 850°C with no hold. (*Continued*.)

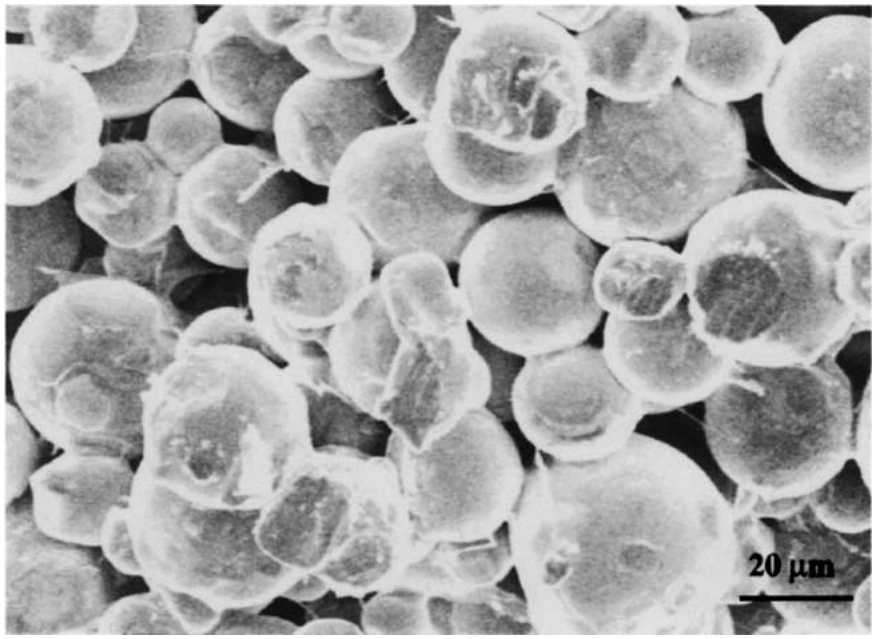

(c)

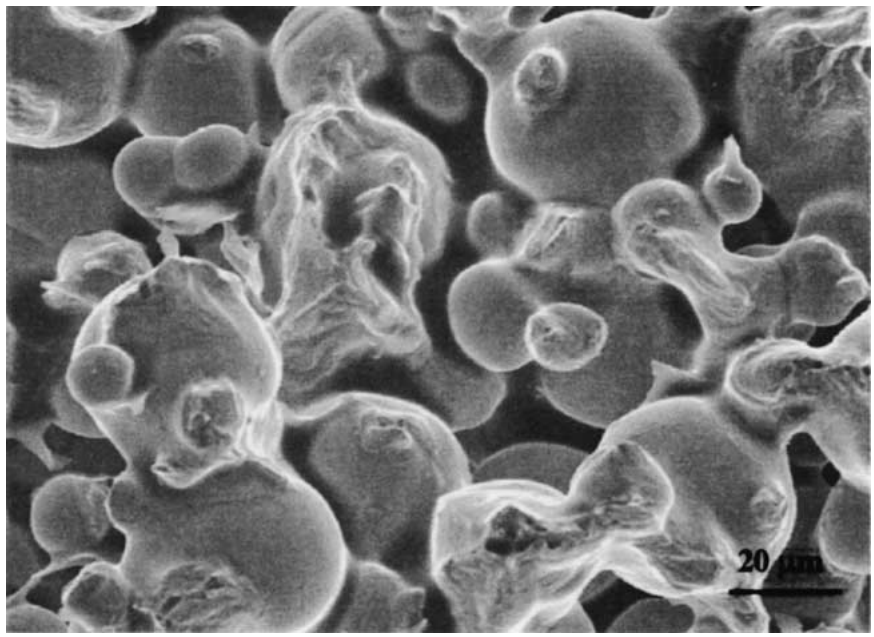

(d)

Figure 10 (*Continued*.)

model to describe *in situ* strength σ_T as a function of sintering parameters as follows:

$$\sigma_T = A\left(\frac{\rho_G}{\rho_A}\right)^n Be^{\frac{Q_A}{RT}} + C\rho_s\left(\frac{X}{D}\right)^2 e^{\frac{Q_S}{RT}} \qquad (3)$$

where A and n are empirical constants, ρ_G and ρ_A are the green and apparent densities, B and Q_A reflect annealing behavior (applicable to compacted powders), while C is a constant that includes the temperature dependent strength of the bulk material, ρ_S is the sintered density, (X/D) is the neck ratio, Q_S is the activation energy for thermal softening, R is the gas constant, and T is the absolute temperature. The first term in Equation 3 accounts for the remaining green strength due to annealing, and the second one combines sintering strengthening and thermal softening effects on strength evolution. Both models demonstrate the importance of bond size on sintered and *in situ* strength.

Fig. 10 shows the progressive neck growth with sintering temperature for bronze. At temperatures below 750°C there was neck growth but little densification. Hence, the sintering strengthening in initial heating is provided by the interparticle neck growth. Although heating to higher temperatures resulted in more neck growth, concomitant thermal softening significantly weakened the compact. This is the reason why the *in situ* strength peaked at about 750°C for the bronze, and decreased at higher temperatures. As evident from Fig. 9, cooling from 800°C, where the strength was 12.8 MPa, to room temperature gives a transverse rupture strength

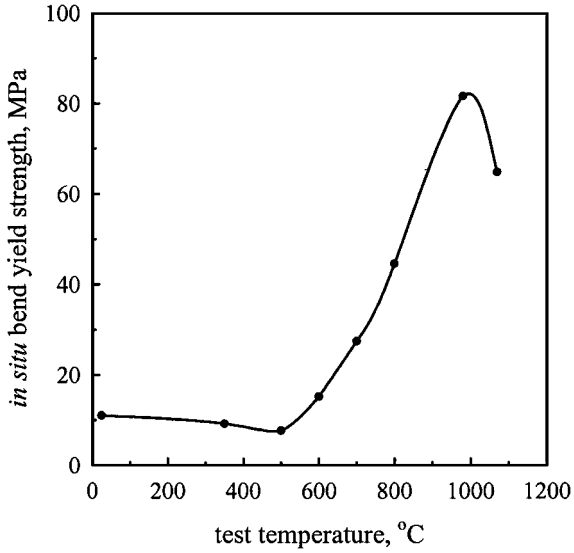

Figure 11 *In situ* bend yield strength versus test temperature for the Fe-2Ni-0.9C steel. The heating rate was 5°C/min with no hold at the test temperature in a mixture of 80% N_2 and 20% H_2.

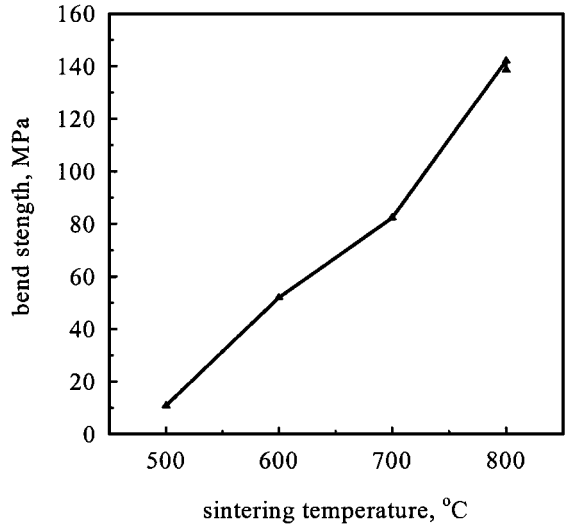

Figure 12 Room temperature bend yield strength versus peak temperature for Fe-2Ni-0.9C steel heated at 5°C/min in an atmosphere of 80% N_2 and 20% H_2.

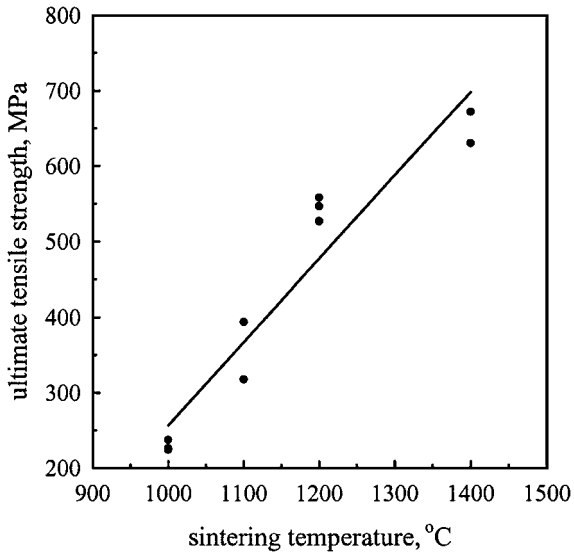

Figure 13 Room temperature ultimate tensile strength versus peak sintering temperature for the Fe-2Ni-0.9C steel heated at 5°C/min in an atmosphere of 80% N_2 and 20% H_2.

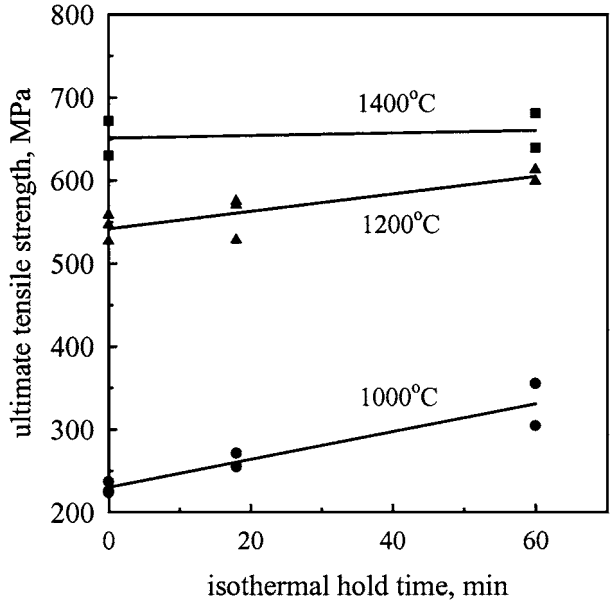

Figure 14 Room temperature ultimate tensile strength versus isothermal hold time for Fe-2Ni-0.9C steel heated at 5°C/min in an atmosphere of 80% N_2 and 20% H_2.

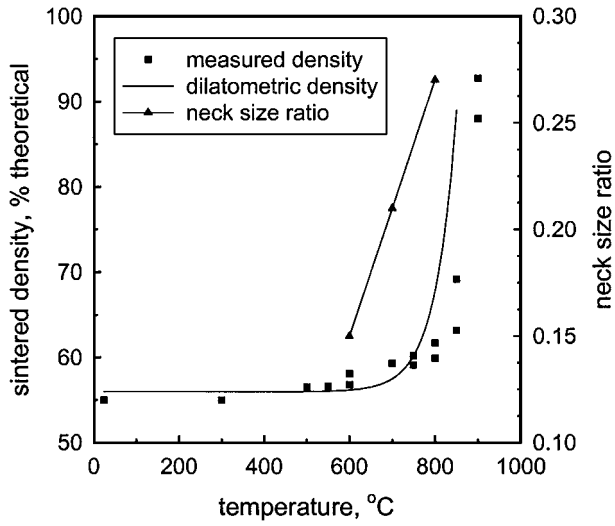

Figure 15 Sintered density and interparticle neck size ratio versus sintering temperature for the Cu-10Sn bronze heated at 5°C/min in hydrogen with no hold at the sintering temperature.

of 161 MPa. Thermal softening was also observed for the steel powder in Fig. 11, in which the *in situ* strength curve peaked at about 970°C and decreased to 62 MPa at 1070°C.

5. Conclusions

The *in situ* strength evolution during sintering is determined by three parameters-interparticle neck growth, compact densification, and bulk material thermal softening. Substantial neck growth occurs during initial heating with little densification, resulting in sinter strengthening. At high temperatures, densification becomes active, further adding to compact strength by the eliminating pores and increasing the particle coordination number (number of bonds per particle). However, at these same high temperatures, bulk material thermal softening leads to significant strength loss. *In situ*

strength evolution in sintering emerges from the competition between interparticle neck growth, densification, and thermal softening. These and other results suggest that sintering densification and compact thermal softening are inherently related. In all cases tested to date, there is a consistent pattern of densification being delayed to a point where thermal softening lowers the *in situ* strength [5].

Acknowledgements

The authors wish to acknowledge the National Aeronautics and Space Administration and the National Science Foundation for financial support on these studies linking densification and distortion during sintering.

References

1. R. M. GERMAN, "Powder Metallurgy Science," 2nd edn. (Metal Powder Industries Federation, Princeton, NJ, 1994).
2. G. A. SHOALS and R. M. GERMAN, *Metall. Mater. Trans. A* **30A** (1999) 465.
3. T. J. WEAVER, M. S. Thesis, The Pennsylvania State University, University Park, PA, 1996.
4. N. E. DOWLING, "Mechanical Behavior of Materials," 2nd edn. (Prentice Hall, Upper Saddle River, NJ, 1998).
5. R. M. GERMAN, *Mater. Trans.* **42** (2001) 1409.
6. A. LAL, J. LIU, G. A. SHOALS and R. M. GERMAN, "Advances in Powder Metallurgy and Particulate Materials" (Metal Powder Industries Federation, NJ, 1998) p. 12.33.
7. A. C. NYCE and W. M. SHAFFER, *Inter. J. Powder Met.* **15** (1972) 171.

Received 28 November 2000
and accepted 28 August 2001